A Multi-Resolution Approach for *BCS*-Based Imaging of Sparse Scatterers

N. Anselmi, L. Poli, G. Oliveri, and A. Massa

Abstract

In this work, a novel Bayesian compressive sensing (*BCS*)-based microwave imaging method is proposed. The developed technique suitably combines the regularization properties of *CS* techniques with those of the iterative multi-scale approach (*IMSA*), in order to exploit the progressively acquired information on the scatterer location and size and improve the overall accuracy of the retrieved images. Toward this end, an innovative information-driven relevance vector machine (*RVM*) has been developed. Some preliminary results are shown to verify the effectiveness of the proposed *IMSA-BCS* strategy.

1 Mathematical Formulation

Let us consider an inaccessible investigation domain Λ irradiated by a set of incident transverse-magnetic planes $E^v_{inc}(\mathbf{r}^v)$, $v = 1, ..., V$, impinging from the angular directions $\theta^v = \frac{2\pi}{V}(v-1)$, being V the number of views. In this working scenario, the scattered field $E^v_{scatt}(\mathbf{r}^v_s)$, $s = 1, ..., S$, is supposed to be measured through a set of S sensors equally displaced on a circular observation domain Θ, external to the investigation domain ($\Lambda \cap \Theta = 0$), having radius ρ. The exact location of the sensors are identified by the position vector $\mathbf{r}^v_s = (\rho \cos\theta^v_s \sin\theta^v_s)$, being $\theta^v_s = \theta^v + \frac{2\pi}{S}(s-1)$.

This scattered field is known to be dependent on the equivalent currents $J^v_{eq}(\mathbf{r})$ generated in the support of the unknown scatterers placed into the domain Λ, according to the *data equation*

$$E^v_{scatt}(\mathbf{r}^v_s) = -k_0^2 \int_\Lambda J^v_{eq}(\mathbf{r}') \, G(\mathbf{r}^v_s/\mathbf{r}') \tag{1}$$

where $G(\mathbf{r}^v_s/\mathbf{r}')$ is the Green's function in the free space and $k_0 = \omega\sqrt{\varepsilon_0\mu_0}$. The material properties of the investigation domain Λ in terms of relative dielectric permittivity $\varepsilon_r(\mathbf{r})$ and electric conductivity $\sigma(\mathbf{r})$ are described by means of the object function

$$\tau(\mathbf{r}) = \varepsilon_r(\mathbf{r}) - \varepsilon_0 - \frac{\sigma(\mathbf{r})}{2\pi f \varepsilon_0} \tag{2}$$

f being the frequency of the TM plane wave.

In order to numerically deal with (1), the investigation domain is discretized into N sub-domains (cells), providing the matrix form of

$$\mathbf{E}^v = \mathbf{G}\mathbf{J}^v_{eq} + \mathbf{N}^v \tag{3}$$

$\mathbf{G}$ being the Green's matrix and $\mathbf{N}^v$ a zero mean additive Gaussian noise vector of variance σ^2. The dielectric features of the N sub-domains described through the discretized form of the object function τ are then retrieved through the following iterative strategy which combines a multi-resolution approach and the BCS method, aimed to maximize the a-posteriori probability of the equivalent sources given the scattered field as:

$$\widehat{\mathbf{J}}^v_{eq} = \arg\left\{\max\left[\mathcal{P}\left(\mathbf{J}^v_{eq}\middle|\,\mathbf{E}^v_{scatt}\right)\right]\right\}, \qquad v = 1, ..., V \tag{4}$$

More in detail, the algorithms works as follows:

1. *Initialization*: Definition of input parameters of the BCS problem, namely the initial estimation of the noise on the scattered data, σ^2_{init}, the convergence parameter, γ, and the parameter related to the stopping criterion of the $IMSA$, χ. Set the region of interest equal to the whole domain $\mathcal{D}^{(1)} = \Lambda$;

2. *BCS inversion via "Constrained-RVM"*:

   (a) increase of the iteration index: $i = i + 1$;

   (b) solution of the BCS problem within the Region of Interest (RoI) $\mathcal{D}^{(i-1)}$ defined at the $(i-1)$-th step, by maximizing the following cost function:

$$\ell\left(\mathbf{a}^{v}\right)=-0.5\left[2S\log\left(2\pi\right)+\log\left(\mathbf{C}\right)+\left(\mathbf{E}_{scatt}^{v}\right)^{T}\mathbf{C}^{-1}\left(\mathbf{E}_{scatt}^{v}\right)\right],\qquad v=1,...,V \tag{5}$$

where $\mathbf{C}=\sigma^{2}\mathbf{I}+\mathbf{G}\left[diag\left(\mathbf{a}^{v}\right)\right]^{-1}\mathbf{G}^{T}$ and being $\mathbf{a}^{v}$ the hyperparameter vector whose entries corresponding to the cells out of the *RoI* $\mathcal{D}^{(i-1)}$ are forced to ∞;

3. *Equivalent Current Retrieval*:

   Computation of the equivalent currents starting from the hyperparameter vector $\mathbf{a}^{v}$ according to:

$$\mathbf{J}_{eq}^{v}=\frac{1}{\sigma^{2}}\left[\frac{\mathbf{G}^{T}\mathbf{G}}{\sigma^{2}}diag\left(\mathbf{a}^{v}\right)\right]^{-1}\mathbf{G}^{T}\mathbf{E}_{scatt}^{v},\qquad v=1,...,V \tag{6}$$

4. *Features' Retrieval*:

   Reconstruction of the material properties of the investigation domain taking advantage from the first order Born approximation through

$$\tau\left(\mathbf{r}_{n}^{(i)}\right)=\frac{1}{V}\sum\frac{\mathbf{J}_{eq}^{v}\left(\mathbf{r}_{n}^{(i)}\right)}{\mathbf{E}_{inc}^{v}\left(\mathbf{r}_{n}^{(i)}\right)},\qquad n=1,...,N \tag{7}$$

   being $\mathbf{r}_{n}^{(i)}$ the barycenter of the n-th cell within the *RoI* $\mathcal{D}^{(i-1)}$;

5. *Convergence Check*:

   Definition of the new *RoI* $\mathcal{D}^{(i)}$ according to the contrast function distribution and evaluation of the following termination condition:

$$\left(\frac{L^{(i-1)}-L^{(i)}}{L^{(i)}}\right)<\chi \tag{8}$$

   being $L^{(i)}$ the side of the *RoI* $\mathcal{D}^{(i)}$. If such a condition is met, then stop the iterative process, otherwise go to step 2.

2 Preliminary Numerical Assessment

2.1 L-shaped Object, $\ell = 1.5\lambda$

Test Case Description

Direct solver:

- Side of the investigation domain: $L = 6.0\lambda$
- Cubic domain divided in $\sqrt{D} \times \sqrt{D}$ cells
- Number of cells for the direct solver: $D = 1600$ (discretization $= \lambda/10$)

Investigation domain:

- Cubic domain divided in $\sqrt{N} \times \sqrt{N}$ cells
- Number of cells for the inversion:
  - First Step IMSA: $N^{(1)} = 100$ (discretization $= \lambda/10$)
  - Following Steps IMSA: $N^{(i)}$ not fixed, defined according to the estimated RoI $\mathcal{D}^{(i)}$

Measurement domain:

- Total number of measurements: $M = 60$
- Measurement points placed on circles of radius $\rho = 4.5\lambda$

Sources:

- Plane waves
- Number of views: $V = 60$; $\theta_{inc}^{v} = 0° + (v-1) \times (360/V)$
- Amplitude: $A = 1.0$
- Frequency: $F = 300$ MHz ($\lambda = 1$)

Background:

- $\varepsilon_r = 1.0$
- $\sigma = 0$ [S/m]

Scatterer

- L-shaped object, $\ell = 1.5\lambda$
- $\varepsilon_r \in \{1.01, 1.02, 1.04, 1.05, 1.06, 1.08, 1.10, 1.15, 1.20\}$
- $\sigma = 0$ [S/m]

2.1.1 L-shaped Object, $\ell = 1.5\lambda$, $\tau = 0.02$ - IMSA-BCS reconstructed profiles

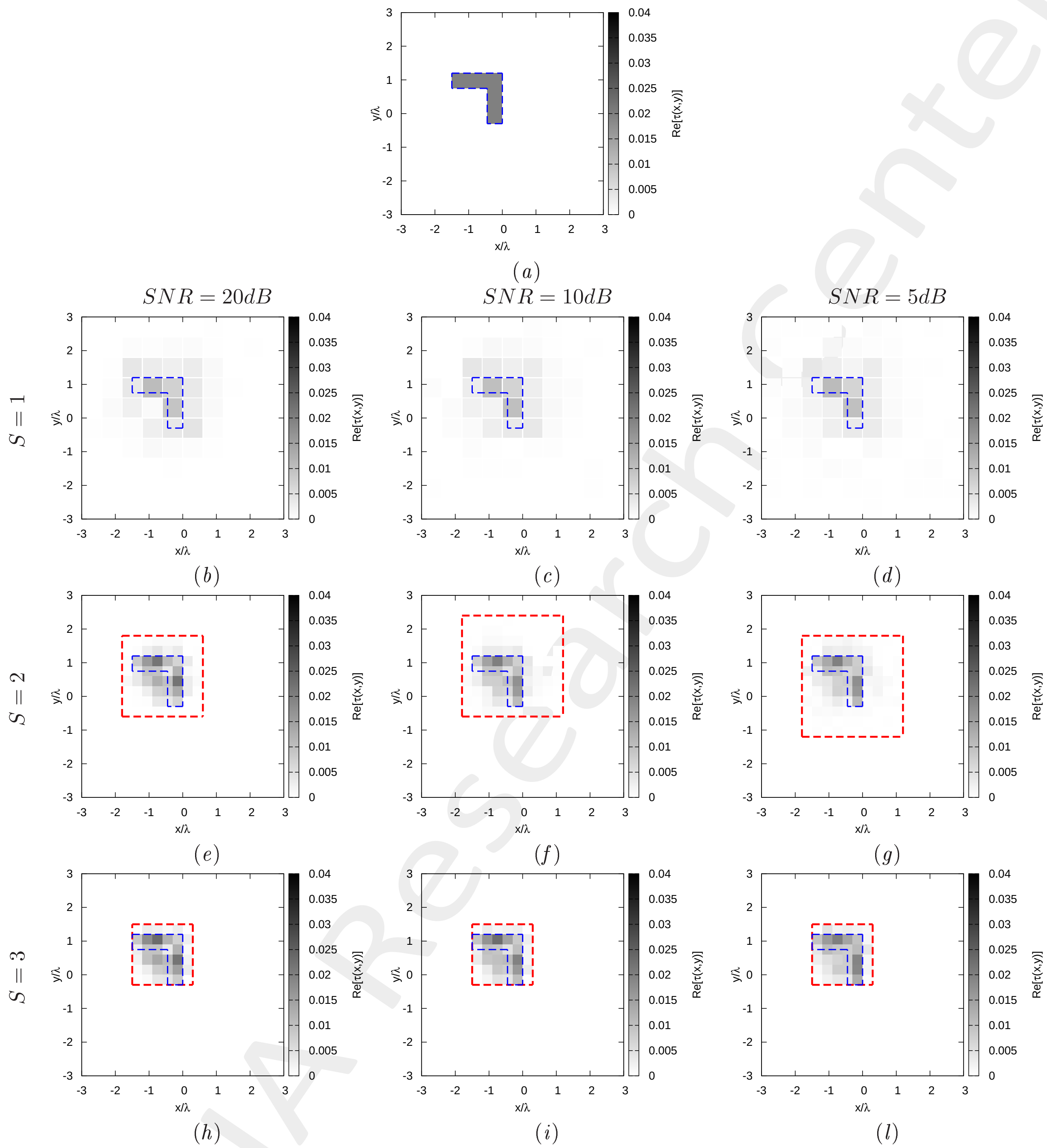

Figure 1: *L-shaped Object*, $\ell = 1.5\lambda$, $\tau = 0.02$ - (a) Actual profile and (b)-(o) IMSA-BCS reconstructed profiles for $(b)(e)(h)$ $SNR = 20$ [dB], $(c)(f)(i)$ $SNR = 10$ [dB] and $(d)(g)(l)$ $SNR = 5$ [dB] at the step (b)-(d) $S = 1$, (e)-(g) $S = 2$, and (h)-(l) $S = 3$.

	$SNR = 50dB$			
	$S=1$	$S=2$	$S=3$	$S=4$
ξ_{tot}	9.01×10^{-4}	5.09×10^{-4}	5.64×10^{-4}	5.64×10^{-4}
ξ_{int}	1.20×10^{-2}	8.97×10^{-3}	1.04×10^{-2}	1.04×10^{-2}
ξ_{ext}	5.30×10^{-4}	2.29×10^{-4}	2.39×10^{-4}	2.39×10^{-4}
	$SNR = 20dB$			
	$S=1$	$S=2$	$S=3$	$S=4$
ξ_{tot}	9.09×10^{-4}	5.21×10^{-4}	4.85×10^{-4}	5.72×10^{-4}
ξ_{int}	1.21×10^{-2}	9.18×10^{-3}	8.73×10^{-3}	1.04×10^{-2}
ξ_{ext}	5.34×10^{-4}	2.35×10^{-4}	2.13×10^{-4}	2.47×10^{-4}
	$SNR = 10dB$			
	$S=1$	$S=2$	$S=3$	$S=4$
ξ_{tot}	9.38×10^{-4}	5.18×10^{-4}	4.69×10^{-4}	5.42×10^{-4}
ξ_{int}	1.22×10^{-2}	8.85×10^{-3}	8.26×10^{-3}	1.01×10^{-2}
ξ_{ext}	5.56×10^{-4}	2.42×10^{-4}	2.12×10^{-4}	2.24×10^{-4}
	$SNR = 5dB$			
	$S=1$	$S=2$	$S=3$	$S=4$
ξ_{tot}	9.73×10^{-4}	5.31×10^{-4}	4.34×10^{-4}	4.34×10^{-4}
ξ_{int}	1.22×10^{-2}	8.84×10^{-3}	7.44×10^{-3}	7.44×10^{-3}
ξ_{ext}	5.85×10^{-4}	2.50×10^{-4}	2.01×10^{-4}	2.01×10^{-4}

Table I: *L-shaped Object*, $\ell = 1.5\lambda$, $\tau = 0.02$ - Reconstruction errors: total (ξ_{tot}), internal (ξ_{int}) and external (ξ_{ext}) errors.

	$SNR = 50dB$			
	$S=1$	$S=2$	$S=3$	$S=4$
$L^{(S)}$	6.00	1.50	1.50	1.50
$N^{(S)}$	100	148	148	148
$Q^{(S)}$	100	64	25	25
	$SNR = 20dB$			
	$S=1$	$S=2$	$S=3$	$S=4$
$L^{(S)}$	6.00	1.50	1.50	1.50
$N^{(S)}$	100	148	148	148
$Q^{(S)}$	100	64	36	25
	$SNR = 10dB$			
	$S=1$	$S=2$	$S=3$	$S=4$
$L^{(S)}$	6.00	1.50	1.50	1.50
$N^{(S)}$	100	175	175	175
$Q^{(S)}$	100	100	36	25
	$SNR = 5dB$			
	$S=1$	$S=2$	$S=3$	$S=4$
$L^{(S)}$	6.00	1.80	1.80	1.80
$N^{(S)}$	100	175	175	175
$Q^{(S)}$	100	100	36	36

Table II: *L-shaped Object*, $\ell = 1.5\lambda$, $\tau = 0.02$ - Investigation domain parameters: restricted investigation domain size $L^{(S)}$, total number of cells $N^{(S)}$ and number of cells within the restricted domain size $Q^{(S)}$.

2.1.2 L-shaped Object, $\ell = 1.5\lambda$, $\tau = 0.05$ - IMSA-BCS reconstructed profiles

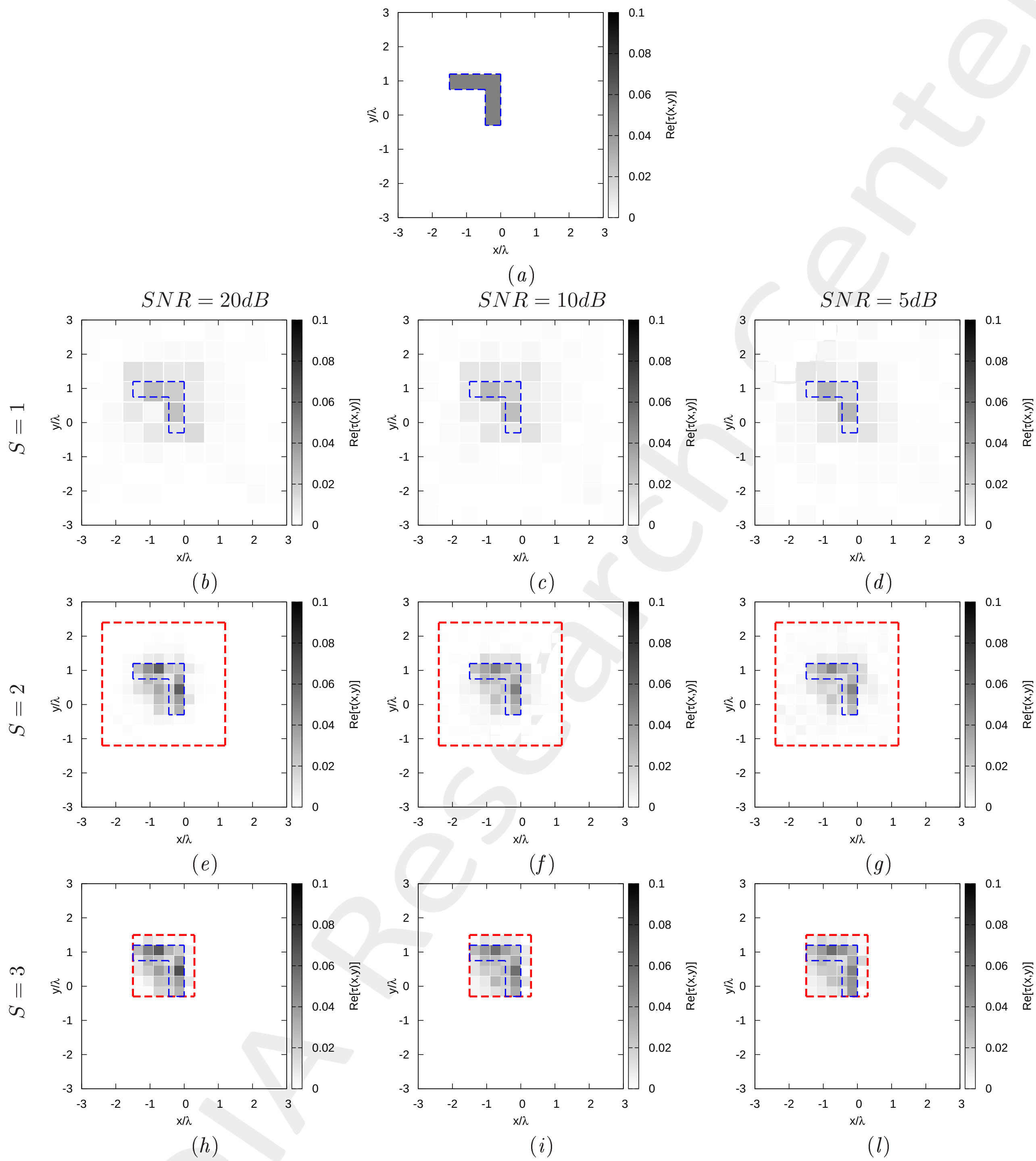

Figure 2: *L-shaped Object*, $\ell = 1.5\lambda$, $\tau = 0.05$ - (a) Actual profile and (b)-(o) IMSA-BCS reconstructed profiles for $(b)(e)(h)$ $SNR = 20$ [dB], $(c)(f)(i)$ $SNR = 10$ [dB] and $(d)(g)(l)$ $SNR = 5$ [dB] at the step (b)-(d) $S = 1$, (e)-(g) $S = 2$, and (h)-(l) $S = 3$.

	$SNR = 50dB$			
	$S=1$	$S=2$	$S=3$	$S=4$
ξ_{tot}	2.75×10^{-3}	1.31×10^{-3}	1.23×10^{-3}	1.23×10^{-3}
ξ_{int}	2.82×10^{-2}	2.00×10^{-2}	1.99×10^{-2}	1.99×10^{-2}
ξ_{ext}	1.87×10^{-3}	6.78×10^{-4}	6.12×10^{-4}	6.12×10^{-4}
	$SNR = 20dB$			
	$S=1$	$S=2$	$S=3$	$S=4$
ξ_{tot}	2.77×10^{-3}	1.39×10^{-3}	1.23×10^{-3}	1.23×10^{-3}
ξ_{int}	2.84×10^{-2}	2.14×10^{-2}	1.98×10^{-2}	1.98×10^{-2}
ξ_{ext}	1.86×10^{-3}	7.21×10^{-4}	6.17×10^{-4}	6.17×10^{-4}
	$SNR = 10dB$			
	$S=1$	$S=2$	$S=3$	$S=4$
ξ_{tot}	2.81×10^{-3}	1.47×10^{-3}	1.19×10^{-3}	1.19×10^{-3}
ξ_{int}	2.83×10^{-2}	1.98×10^{-2}	1.74×10^{-2}	1.74×10^{-2}
ξ_{ext}	1.87×10^{-3}	8.23×10^{-4}	6.50×10^{-4}	6.50×10^{-4}
	$SNR = 5dB$			
	$S=1$	$S=2$	$S=3$	$S=4$
ξ_{tot}	2.93×10^{-3}	1.67×10^{-3}	1.19×10^{-3}	1.19×10^{-3}
ξ_{int}	2.82×10^{-2}	2.20×10^{-2}	1.66×10^{-2}	1.66×10^{-2}
ξ_{ext}	1.98×10^{-3}	9.33×10^{-4}	6.73×10^{-4}	6.73×10^{-4}

Table III: *L-shaped Object*, $\ell = 1.5\lambda$, $\tau = 0.05$ - Reconstruction errors: total (ξ_{tot}), internal (ξ_{int}) and external (ξ_{ext}) errors.

	$SNR = 50dB$			
	$S=1$	$S=2$	$S=3$	$S=4$
$L^{(S)}$	6.00	1.80	1.80	1.80
$N^{(S)}$	100	208	208	208
$Q^{(S)}$	100	144	36	36
	$SNR = 20dB$			
	$S=1$	$S=2$	$S=3$	$S=4$
$L^{(S)}$	6.00	1.80	1.80	1.80
$N^{(S)}$	100	208	208	208
$Q^{(S)}$	100	144	36	36
	$SNR = 10dB$			
	$S=1$	$S=2$	$S=3$	$S=4$
$L^{(S)}$	6.00	1.80	1.80	1.80
$N^{(S)}$	100	208	208	208
$Q^{(S)}$	100	144	36	36
	$SNR = 5dB$			
	$S=1$	$S=2$	$S=3$	$S=4$
$L^{(S)}$	6.00	1.80	1.80	1.80
$N^{(S)}$	100	208	208	208
$Q^{(S)}$	100	144	36	36

Table IV: *L-shaped Object*, $\ell = 1.5\lambda$, $\tau = 0.05$ - Investigation domain parameters: restricted investigation domain size $L^{(S)}$, total number of cells $N^{(S)}$ and number of cells within the restricted domain size $Q^{(S)}$.

2.1.3 L-shaped Object, $\ell = 1.5\lambda$, $\tau = 0.10$ - IMSA-BCS reconstructed profiles

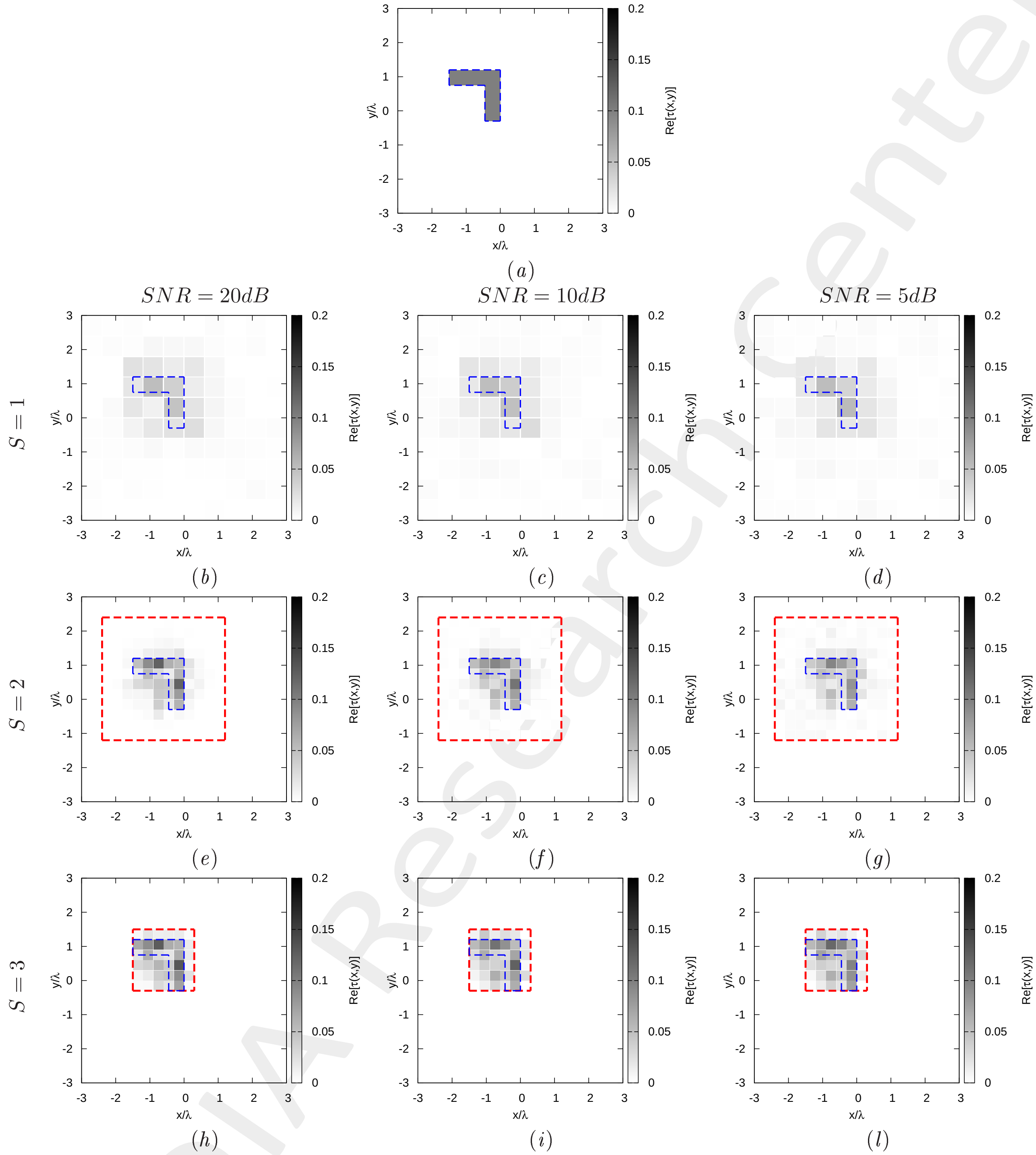

Figure 3: *L-shaped Object*, $\ell = 1.5\lambda$, $\tau = 0.10$ - (a) Actual profile and (b)-(o) IMSA-BCS reconstructed profiles for $(b)(e)(h)$ $SNR = 20$ [dB], $(c)(f)(i)$ $SNR = 10$ [dB] and $(d)(g)(l)$ $SNR = 5$ [dB] at the step (b)-(d) $S = 1$, (e)-(g) $S = 2$, and (h)-(l) $S = 3$.

	$SNR = 50dB$			
	$S = 1$	$S = 2$	$S = 3$	$S = 4$
ξ_{tot}	5.91×10^{-3}	2.63×10^{-3}	2.36×10^{-3}	2.36×10^{-3}
ξ_{int}	5.53×10^{-2}	3.67×10^{-2}	3.50×10^{-2}	3.50×10^{-2}
ξ_{ext}	4.05×10^{-3}	1.40×10^{-3}	1.21×10^{-3}	1.21×10^{-3}
	$SNR = 20dB$			
	$S = 1$	$S = 2$	$S = 3$	$S = 4$
ξ_{tot}	5.89×10^{-3}	2.85×10^{-3}	2.42×10^{-3}	2.42×10^{-3}
ξ_{int}	5.55×10^{-2}	3.99×10^{-2}	3.57×10^{-2}	3.57×10^{-2}
ξ_{ext}	4.03×10^{-3}	1.51×10^{-3}	1.25×10^{-3}	1.25×10^{-3}
	$SNR = 10dB$			
	$S = 1$	$S = 2$	$S = 3$	$S = 4$
ξ_{tot}	5.97×10^{-3}	2.91×10^{-3}	2.55×10^{-3}	2.55×10^{-3}
ξ_{int}	5.49×10^{-2}	3.67×10^{-2}	3.55×10^{-2}	3.55×10^{-2}
ξ_{ext}	4.06×10^{-3}	1.64×10^{-3}	1.39×10^{-3}	1.39×10^{-3}
	$SNR = 5dB$			
	$S = 1$	$S = 2$	$S = 3$	$S = 4$
ξ_{tot}	6.34×10^{-3}	3.91×10^{-3}	2.47×10^{-3}	2.47×10^{-3}
ξ_{int}	5.49×10^{-2}	$NaN \times 10^{-a}$	3.22×10^{-2}	3.22×10^{-2}
ξ_{ext}	4.22×10^{-3}	3.66×10^{-3}	1.36×10^{-3}	1.36×10^{-3}

Table V: *L-shaped Object,* $\ell = 1.5\lambda$, $\tau = 0.10$ - Reconstruction errors: total (ξ_{tot}), internal (ξ_{int}) and external (ξ_{ext}) errors.

	$SNR = 50dB$			
	$S = 1$	$S = 2$	$S = 3$	$S = 4$
$L^{(S)}$	6.00	1.80	1.80	1.80
$N^{(S)}$	100	208	208	208
$Q^{(S)}$	100	144	36	36
	$SNR = 20dB$			
	$S = 1$	$S = 2$	$S = 3$	$S = 4$
$L^{(S)}$	6.00	1.80	1.80	1.80
$N^{(S)}$	100	208	208	208
$Q^{(S)}$	100	144	36	36
	$SNR = 10dB$			
	$S = 1$	$S = 2$	$S = 3$	$S = 4$
$L^{(S)}$	6.00	1.80	1.80	1.80
$N^{(S)}$	100	208	208	208
$Q^{(S)}$	100	144	36	36
	$SNR = 5dB$			
	$S = 1$	$S = 2$	$S = 3$	$S = 4$
$L^{(S)}$	6.00	1.80	1.80	1.80
$N^{(S)}$	100	208	208	208
$Q^{(S)}$	100	144	36	36

Table VI: *L-shaped Object,* $\ell = 1.5\lambda$, $\tau = 0.10$ - Investigation domain parameters: restricted investigation domain size $L^{(S)}$, total number of cells $N^{(S)}$ and number of cells within the restricted domain size $Q^{(S)}$.

2.1.4 L-shaped Object, $\ell = 1.5\lambda$, $\tau = 0.15$ - IMSA-BCS reconstructed profiles

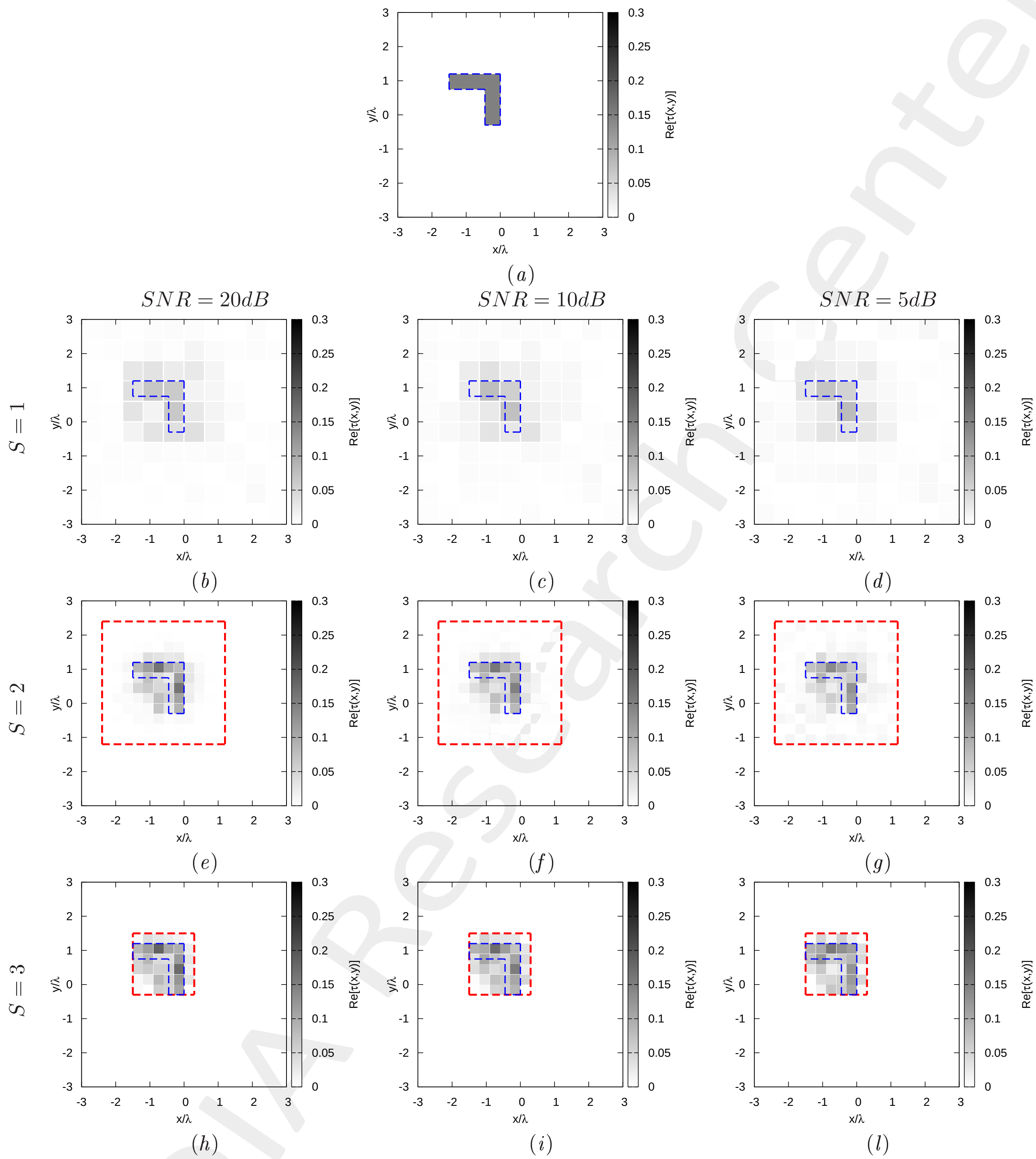

Figure 4: *L-shaped Object*, $\ell = 1.5\lambda$, $\tau = 0.15$ - (a) Actual profile and (b)-(o) IMSA-BCS reconstructed profiles for $(b)(e)(h)$ $SNR = 20$ [dB], $(c)(f)(i)$ $SNR = 10$ [dB] and $(d)(g)(l)$ $SNR = 5$ [dB] at the step (b)-(d) $S = 1$, (e)-(g) $S = 2$, and (h)-(l) $S = 3$.

	$SNR = 50dB$			
	$S = 1$	$S = 2$	$S = 3$	$S = 4$
ξ_{tot}	8.88×10^{-3}	4.04×10^{-3}	3.48×10^{-3}	3.48×10^{-3}
ξ_{int}	8.11×10^{-2}	5.20×10^{-2}	4.62×10^{-2}	4.62×10^{-2}
ξ_{ext}	6.00×10^{-3}	2.17×10^{-3}	1.79×10^{-3}	1.79×10^{-3}
	$SNR = 20dB$			
	$S = 1$	$S = 2$	$S = 3$	$S = 4$
ξ_{tot}	8.92×10^{-3}	4.26×10^{-3}	3.69×10^{-3}	3.69×10^{-3}
ξ_{int}	8.01×10^{-2}	5.46×10^{-2}	4.97×10^{-2}	4.97×10^{-2}
ξ_{ext}	5.97×10^{-3}	2.33×10^{-3}	1.92×10^{-3}	1.92×10^{-3}
	$SNR = 10dB$			
	$S = 1$	$S = 2$	$S = 3$	$S = 4$
ξ_{tot}	9.16×10^{-3}	4.68×10^{-3}	3.87×10^{-3}	3.87×10^{-3}
ξ_{int}	8.02×10^{-2}	5.41×10^{-2}	5.03×10^{-2}	5.03×10^{-2}
ξ_{ext}	6.17×10^{-3}	2.59×10^{-3}	2.10×10^{-3}	2.10×10^{-3}
	$SNR = 5dB$			
	$S = 1$	$S = 2$	$S = 3$	$S = 4$
ξ_{tot}	1.02×10^{-2}	5.50×10^{-3}	3.85×10^{-3}	3.85×10^{-3}
ξ_{int}	7.92×10^{-2}	6.05×10^{-2}	4.50×10^{-2}	4.50×10^{-2}
ξ_{ext}	6.81×10^{-3}	3.12×10^{-3}	2.06×10^{-3}	2.06×10^{-3}

Table VII: *L-shaped Object,* $\ell = 1.5\lambda$, $\tau = 0.10$ - Reconstruction errors: total (ξ_{tot}), internal (ξ_{int}) and external (ξ_{ext}) errors.

	$SNR = 50dB$			
	$S = 1$	$S = 2$	$S = 3$	$S = 4$
$L^{(S)}$	6.00	1.80	1.80	1.80
$N^{(S)}$	100	208	208	208
$Q^{(S)}$	100	144	36	36
	$SNR = 20dB$			
	$S = 1$	$S = 2$	$S = 3$	$S = 4$
$L^{(S)}$	6.00	1.80	1.80	1.80
$N^{(S)}$	100	208	208	208
$Q^{(S)}$	100	144	36	36
	$SNR = 10dB$			
	$S = 1$	$S = 2$	$S = 3$	$S = 4$
$L^{(S)}$	6.00	1.80	1.80	1.80
$N^{(S)}$	100	208	208	208
$Q^{(S)}$	100	144	36	36
	$SNR = 5dB$			
	$S = 1$	$S = 2$	$S = 3$	$S = 4$
$L^{(S)}$	6.00	1.80	1.80	1.80
$N^{(S)}$	100	208	208	208
$Q^{(S)}$	100	144	36	36

Table VIII: *L-shaped Object,* $\ell = 1.5\lambda$, $\tau = 0.15$ - Investigation domain parameters: restricted investigation domain size $L^{(S)}$, total number of cells $N^{(S)}$ and number of cells within the restricted domain size $Q^{(S)}$.

2.1.5 L-shaped Object, $\ell = 1.5\lambda$, $\tau = 0.20$ - IMSA-BCS reconstructed profiles

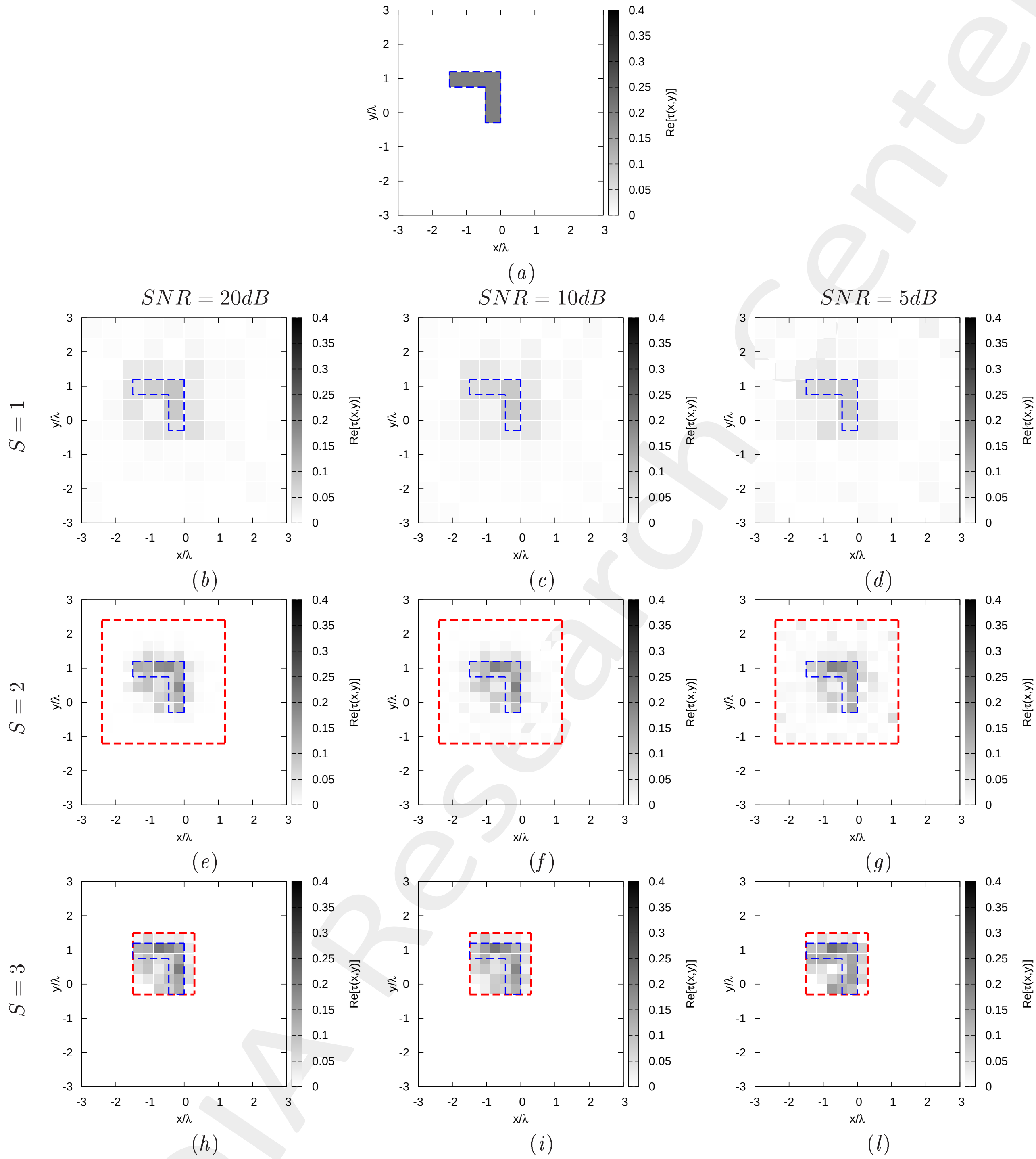

Figure 5: *L-shaped Object*, $\ell = 1.5\lambda$, $\tau = 0.20$ - (a) Actual profile and (b)-(o) IMSA-BCS reconstructed profiles for $(b)(e)(h)$ $SNR = 20$ [dB], $(c)(f)(i)$ $SNR = 10$ [dB] and $(d)(g)(l)$ $SNR = 5$ [dB] at the step (b)-(d) $S = 1$, (e)-(g) $S = 2$, and (h)-(l) $S = 3$.

	$SNR = 50dB$			
	$S = 1$	$S = 2$	$S = 3$	$S = 4$
ξ_{tot}	1.21×10^{-2}	6.02×10^{-3}	4.90×10^{-3}	4.90×10^{-3}
ξ_{int}	1.07×10^{-1}	7.30×10^{-2}	5.81×10^{-2}	5.81×10^{-2}
ξ_{ext}	8.04×10^{-3}	3.23×10^{-3}	2.58×10^{-3}	2.58×10^{-3}
	$SNR = 20dB$			
	$S = 1$	$S = 2$	$S = 3$	$S = 4$
ξ_{tot}	1.19×10^{-2}	5.81×10^{-3}	4.83×10^{-3}	4.83×10^{-3}
ξ_{int}	1.03×10^{-1}	6.95×10^{-2}	5.87×10^{-2}	5.87×10^{-2}
ξ_{ext}	7.98×10^{-3}	3.13×10^{-3}	2.51×10^{-3}	2.51×10^{-3}
	$SNR = 10dB$			
	$S = 1$	$S = 2$	$S = 3$	$S = 4$
ξ_{tot}	1.27×10^{-2}	6.40×10^{-3}	5.23×10^{-3}	5.23×10^{-3}
ξ_{int}	1.07×10^{-1}	7.19×10^{-2}	6.41×10^{-2}	6.41×10^{-2}
ξ_{ext}	8.49×10^{-3}	3.47×10^{-3}	2.75×10^{-3}	2.75×10^{-3}
	$SNR = 5dB$			
	$S = 1$	$S = 2$	$S = 3$	$S = 4$
ξ_{tot}	1.44×10^{-2}	8.26×10^{-3}	5.85×10^{-3}	5.85×10^{-3}
ξ_{int}	1.06×10^{-1}	7.72×10^{-2}	5.98×10^{-2}	5.98×10^{-2}
ξ_{ext}	9.55×10^{-3}	4.70×10^{-3}	3.09×10^{-3}	3.09×10^{-3}

Table IX: *L-shaped Object*, $\ell = 1.5\lambda$, $\tau = 0.20$ - Reconstruction errors: total (ξ_{tot}), internal (ξ_{int}) and external (ξ_{ext}) errors.

	$SNR = 50dB$			
	$S = 1$	$S = 2$	$S = 3$	$S = 4$
$L^{(S)}$	6.00	1.80	1.80	1.80
$N^{(S)}$	100	208	208	208
$Q^{(S)}$	100	144	36	36
	$SNR = 20dB$			
	$S = 1$	$S = 2$	$S = 3$	$S = 4$
$L^{(S)}$	6.00	1.80	1.80	1.80
$N^{(S)}$	100	208	208	208
$Q^{(S)}$	100	144	36	36
	$SNR = 10dB$			
	$S = 1$	$S = 2$	$S = 3$	$S = 4$
$L^{(S)}$	6.00	1.80	1.80	1.80
$N^{(S)}$	100	208	208	208
$Q^{(S)}$	100	144	36	36
	$SNR = 5dB$			
	$S = 1$	$S = 2$	$S = 3$	$S = 4$
$L^{(S)}$	6.00	1.80	1.80	1.80
$N^{(S)}$	100	208	208	208
$Q^{(S)}$	100	144	36	36

Table X: *L-shaped Object*, $\ell = 1.5\lambda$, $\tau = 0.20$ - Investigation domain parameters: restricted investigation domain size $L^{(S)}$, total number of cells $N^{(S)}$ and number of cells within the restricted domain size $Q^{(S)}$.

2.1.6 L-shaped Object, $\ell = 1.5\lambda$, $\tau = 0.20$ - IMSA-BCS multi-resolution grids

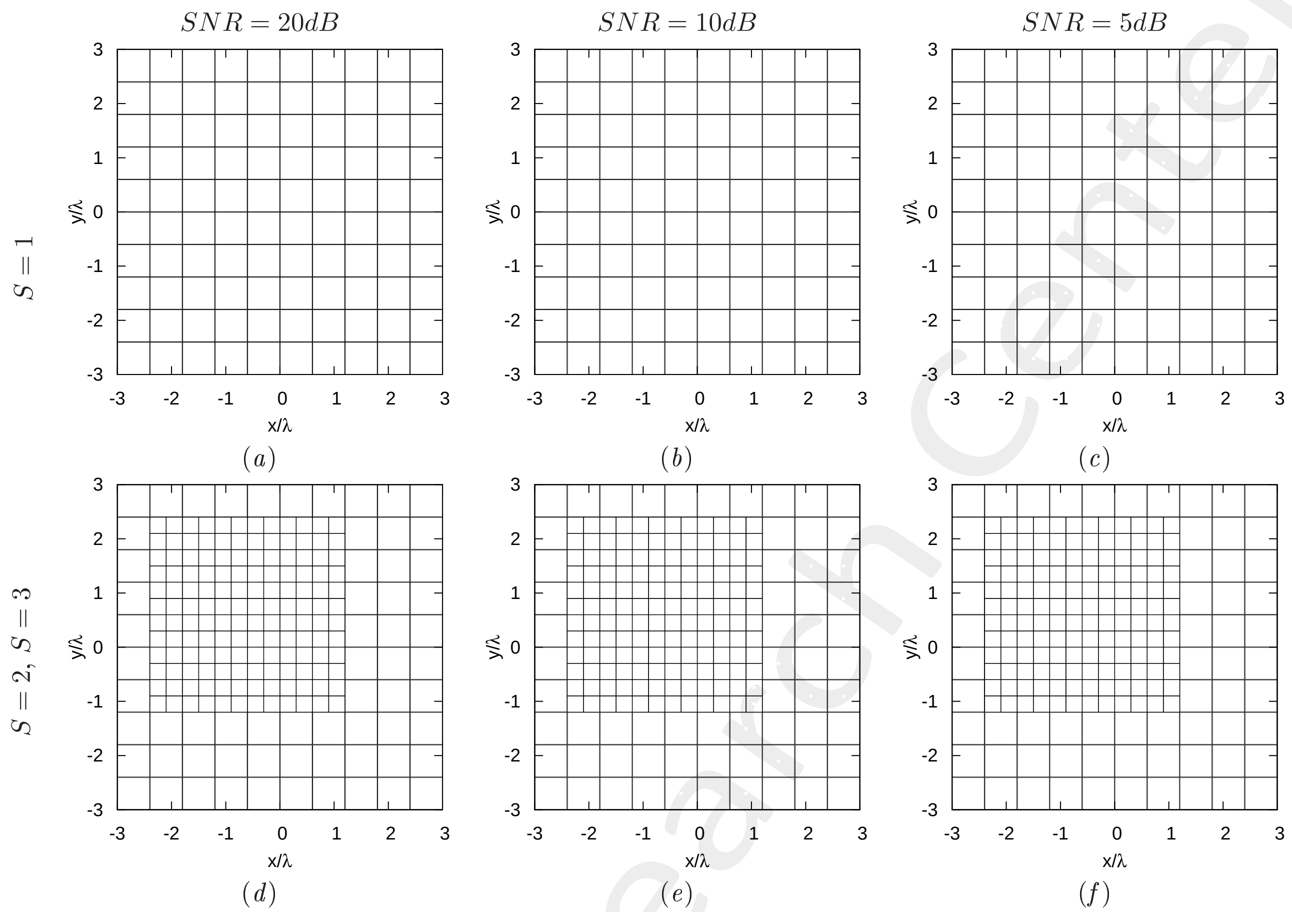

Figure 6: *L-shaped Object*, $\ell = 1.5\lambda$, $\tau = 0.20$ - Example of IMSA-BCS multi-resolution grids for $(a)(d)$ $SNR = 20$ [dB], $(b)(e)$ $SNR = 10$ [dB] and $(c)(f)$ $SNR = 5$ [dB] at the step (a)-(c) $S = 1$ and (d)-(f) $S = 2$, 3.

2.1.7 L-shaped Object, $\ell = 1.5\lambda$ - Resume: Errors vs. τ

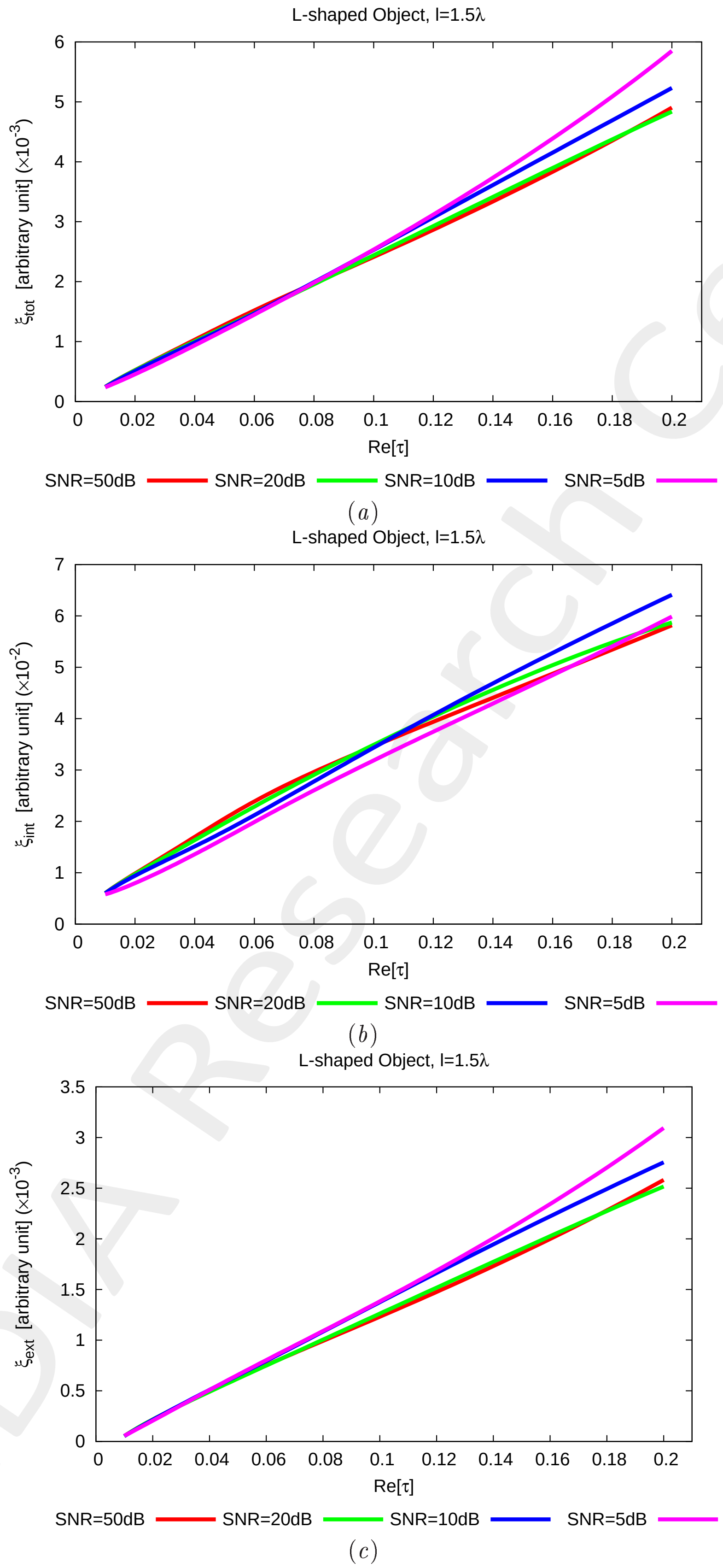

Figure 7: *L-shaped Object*, $\ell = 1.5\lambda$ - Reconstruction errors vs. τ: (a) total error, (b) internal error and (c) external error.

2.1.8 L-shaped Object, $\ell = 1.5\lambda$ - Resume: Errors vs. SNR

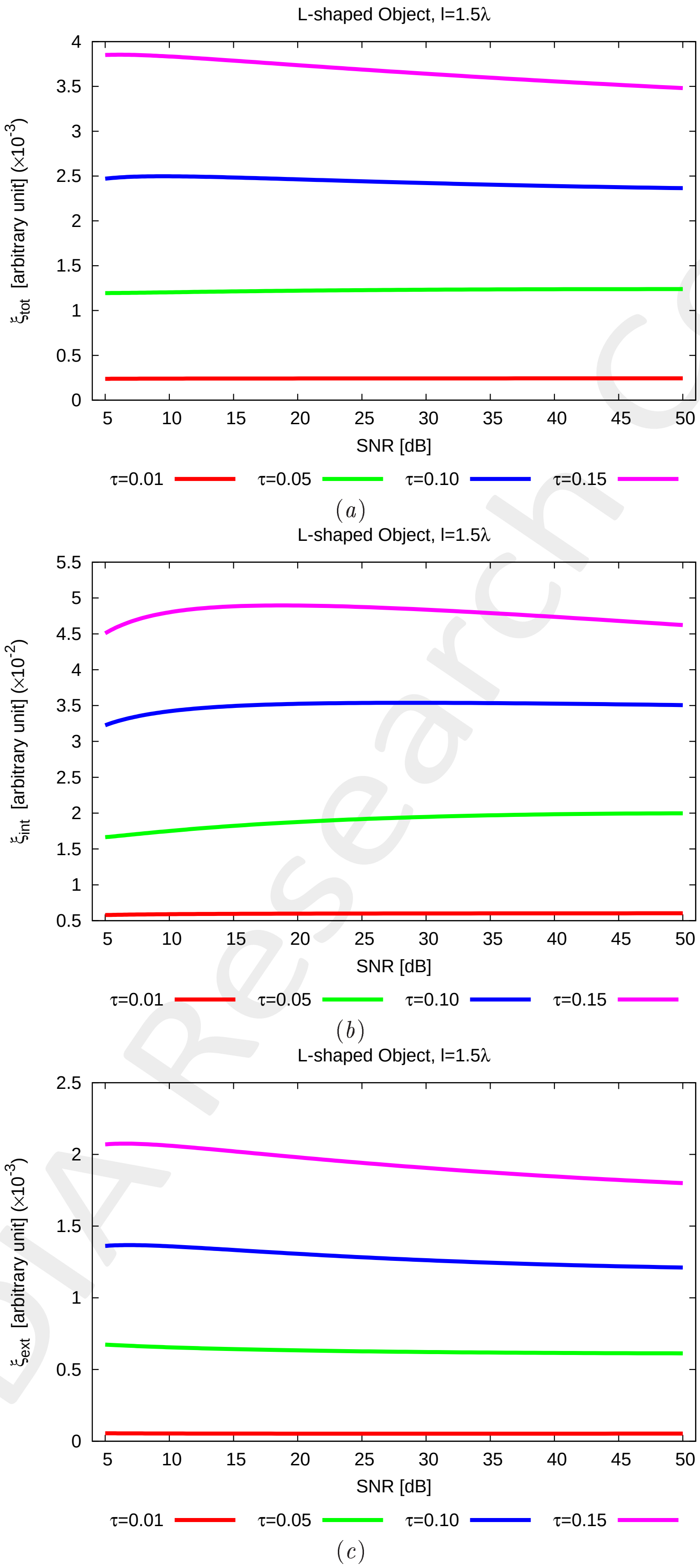

Figure 8: *L-shaped Object*, $\ell = 1.5\lambda$ - Reconstruction errors vs. SNR: (a) total error, (b) internal error and (c) external error.

2.1.9 L-shaped Object, $\ell = 1.5\lambda$ - Resume: Errors vs. $IMSA$ step, S

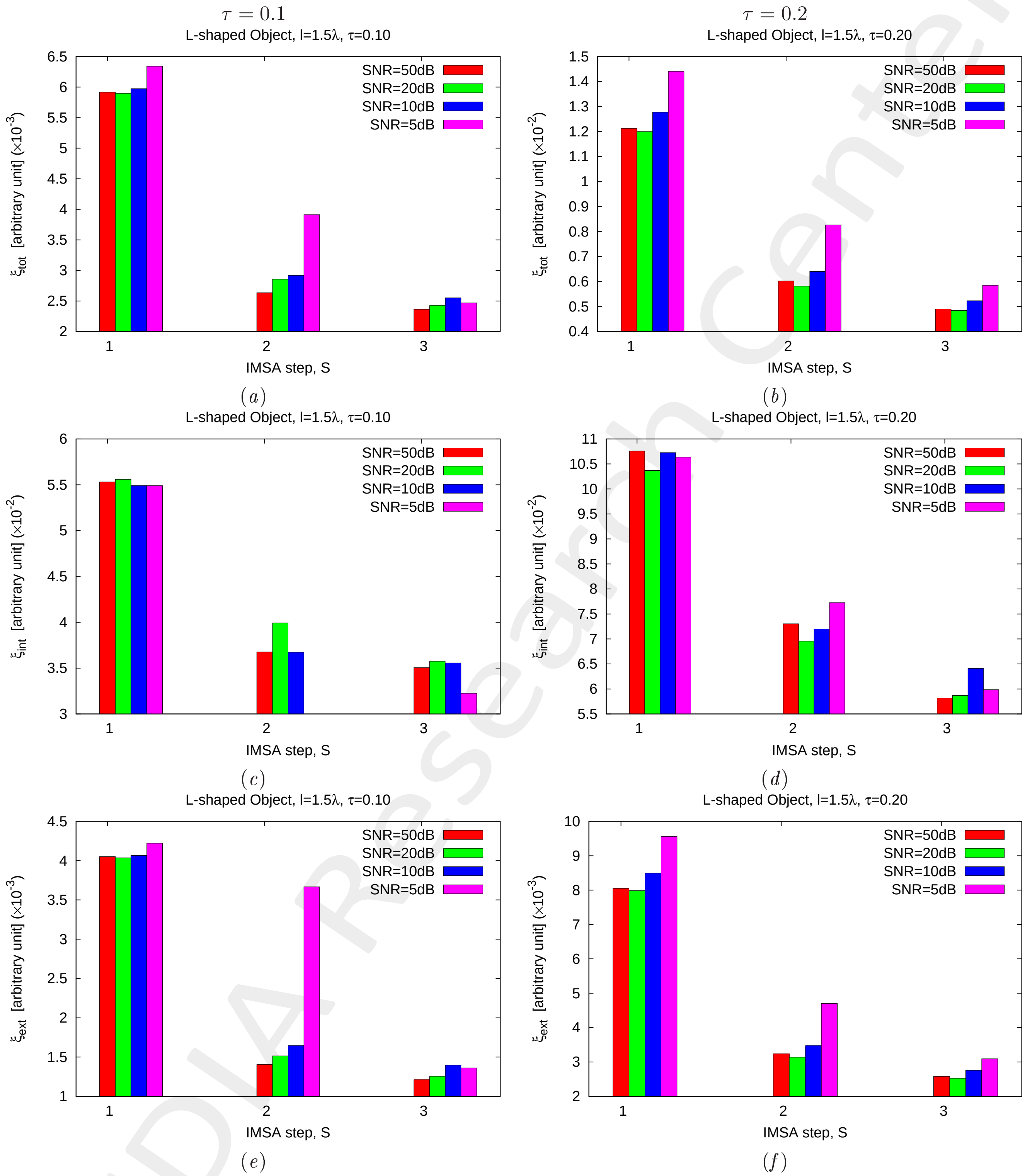

Figure 9: *L-shaped Object*, $\ell = 1.5\lambda$ - Reconstruction errors vs. $IMSA$ step, S: $(a)(b)$ total error, $(c)(d)$ internal error and $(e)(f)$ external error for $(a)(c)(e)$ $\tau = 0.1$ and $(b)(d)(f)$ $\tau = 0.2$.

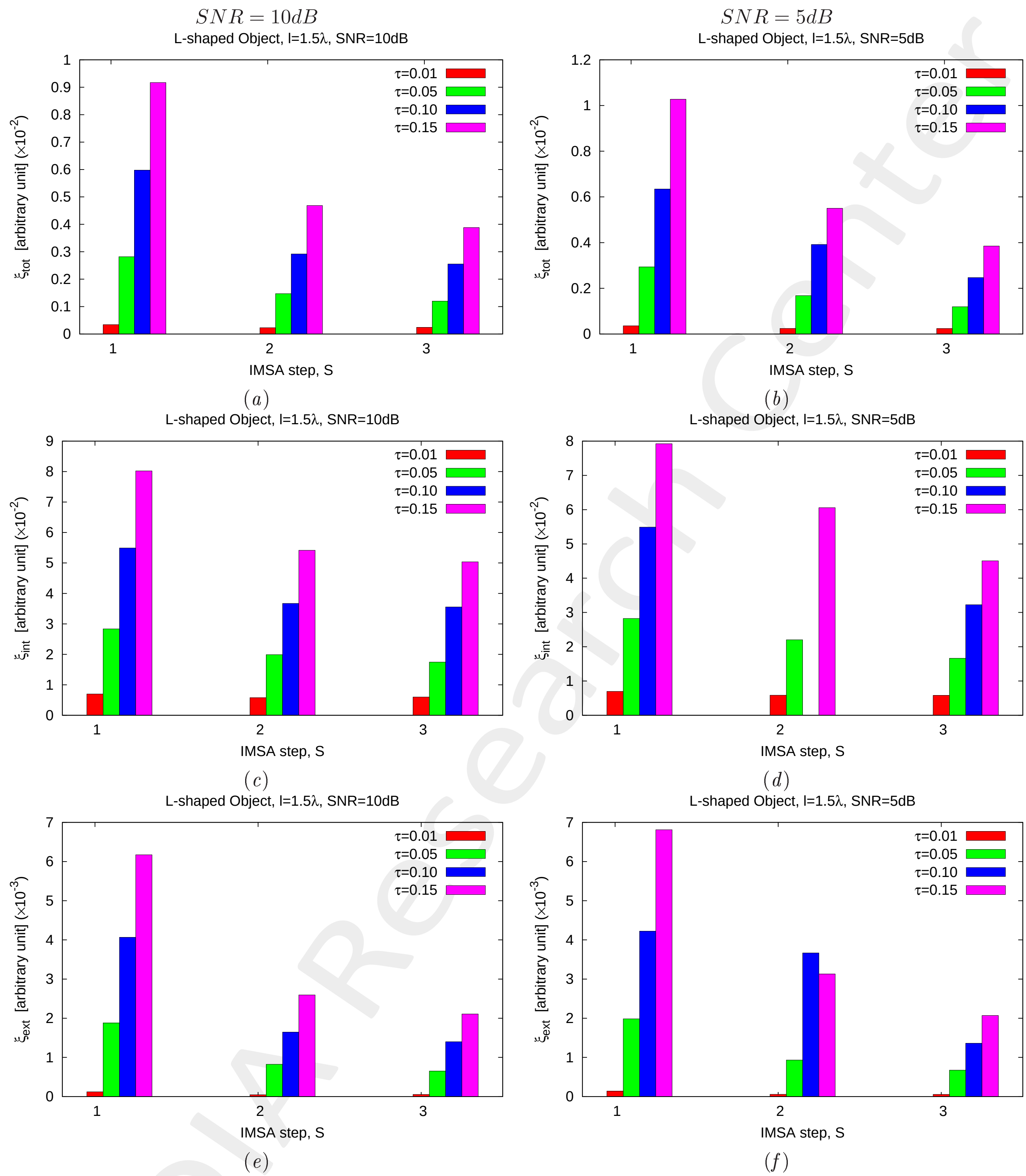

Figure 10: *L-shaped Object*, $\ell = 1.5\lambda$ - Reconstruction errors vs. $IMSA$ step, S: $(a)(b)$ total error, $(c)(d)$ internal error and $(e)(f)$ external error for $(a)(c)(e)$ $SNR = 10dB$ and $(b)(d)(f)$ $SNR = 5dB$.

References

[1] M. Salucci, G. Oliveri, and A. Massa, "GPR prospecting through an inverse scattering frequency-hopping multi-focusing approach," *IEEE Trans. Geosci. Remote Sens.*, vol. 53, no. 12, pp. 6573-6592, Dec. 2015.

[2] M. Salucci, L. Poli, N. Anselmi, and A. Massa, "Multifrequency Particle Swarm Optimization for enhanced multiresolution GPR microwave imaging," *IEEE Trans. Geosci. Remote Sens.*, vol. 55, no. 3, pp. 1305-1317, Mar. 2017.

[3] M. Salucci, L. Poli, and A. Massa, "Advanced multi-frequency GPR data processing for non-linear deterministic imaging," *Signal Processing* - Special Issue on 'Advanced Ground-Penetrating Radar Signal-Processing Techniques,' vol. 132, pp. 306-318, Mar. 2017.

[4] N. Anselmi, G. Oliveri, M. Salucci, and A. Massa, "Wavelet-based compressive imaging of sparse targets," *IEEE Trans. Antennas Propag.*, vol. 63, no. 11, pp. 4889-4900, Nov. 2015.

[5] G. Oliveri, M. Salucci, N. Anselmi, and A. Massa, "Compressive sensing as applied to inverse problems for imaging: theory, applications, current trends, and open challenges," *IEEE Antennas Propag. Mag.* - Special Issue on "Electromagnetic Inverse Problems for Sensing and Imaging," vol. 59, no. 5, pp. 34-46, Oct. 2017.

[6] A. Massa, P. Rocca, and G. Oliveri, "Compressive sensing in electromagnetics - A review," *IEEE Antennas Propag. Mag.*, pp. 224-238, vol. 57, no. 1, Feb. 2015.

[7] N. Anselmi, L. Poli, G. Oliveri, and A. Massa, "Iterative multi-resolution bayesian CS for microwave imaging," *IEEE Trans. Antennas Propag.*, vol. 66, no. 7, pp. 3665-3677, Jul. 2018.

[8] N. Anselmi, G. Oliveri, M. A. Hannan, M. Salucci, and A. Massa, "Color compressive sensing imaging of arbitrary-shaped scatterers," *IEEE Trans. Microw. Theory Techn.*, vol. 65, no. 6, pp. 1986-1999, Jun. 2017.

[9] G. Oliveri, N. Anselmi, and A. Massa, "Compressive sensing imaging of non-sparse 2D scatterers by a total-variation approach within the Born approximation," *IEEE Trans. Antennas Propag.*, vol. 62, no. 10, pp. 5157-5170, Oct. 2014.

[10] L. Poli, G. Oliveri, and A. Massa, "Imaging sparse metallic cylinders through a local shape function Bayesian compressive sensing approach," *Journal of Optical Society of America A*, vol. 30, no. 6, pp. 1261-1272, 2013.

[11] L. Poli, G. Oliveri, F. Viani, and A. Massa, "MT-BCS-based microwave imaging approach through minimum-norm current expansion," *IEEE Trans. Antennas Propag.*, vol. 61, no. 9, pp. 4722-4732, Sep. 2013.

[12] F. Viani, L. Poli, G. Oliveri, F. Robol, and A. Massa, "Sparse scatterers imaging through approximated multitask compressive sensing strategies," *Microwave Opt. Technol. Lett.*, vol. 55, no. 7, pp. 1553-1558, Jul. 2013.

[13] L. Poli, G. Oliveri, P. Rocca, and A. Massa, "Bayesian compressive sensing approaches for the reconstruction of two-dimensional sparse scatterers under TE illumination," *IEEE Trans. Geosci. Remote Sens.*, vol. 51, no. 5, pp. 2920-2936, May 2013.

[14] L. Poli, G. Oliveri, and A. Massa, "Microwave imaging within the first-order Born approximation by means of the contrast-field Bayesian compressive sensing," *IEEE Trans. Antennas Propag.*, vol. 60, no. 6, pp. 2865-2879, Jun. 2012.

[15] G. Oliveri, L. Poli, P. Rocca, and A. Massa, "Bayesian compressive optical imaging within the Rytov approximation," *Optics Letters*, vol. 37, no. 10, pp. 1760-1762, 2012.

[16] G. Oliveri, P. Rocca, and A. Massa, "A Bayesian compressive sampling-based inversion for imaging sparse scatterers," *IEEE Trans. Geosci. Remote Sens.*, vol. 49, no. 10, pp. 3993-4006, Oct. 2011.

[17] G. Oliveri, M. Salucci, and N. Anselmi, "Tomographic imaging of sparse low-contrast targets in harsh environments through matrix completion," *IEEE Trans. Microw. Theory Tech.*, vol. 66, no. 6, pp. 2714-2730, Jun. 2018.

[18] M. Salucci, A. Gelmini, L. Poli, G. Oliveri, and A. Massa, "Progressive compressive sensing for exploiting frequency-diversity in GPR imaging," *Journal of Electromagnetic Waves and Applications*, vol. 32, no. 9, pp. 1164- 1193, 2018.